Lawrence Berkeley Laboratory
UNIVERSITY OF CALIFORNIA

Materials & Molecular
Research Division

Submitted to Metal Science

THEORETICAL DIFFUSION PROFILES IN SINGLE PHASE TERNARY SYSTEMS

G. W. Roper and D. P. Whittle

February 1980

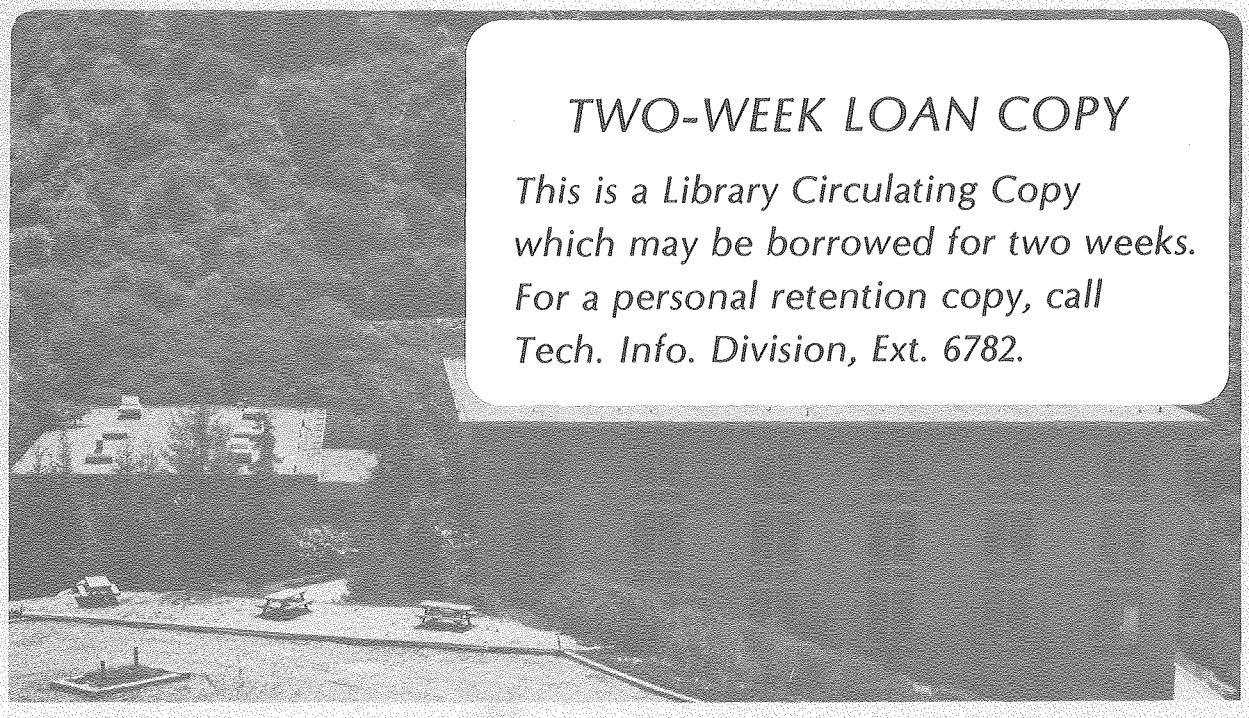

Prepared for the U.S. Department of Energy under Contract W-7405-ENG-48

DISCLAIMER

THEORETICAL DIFFUSION PROFILES IN SINGLE PHASE TERNARY SYSTEMS

G. W. Roper* and D. P. Whittle

Lawrence Berkeley Laboratory

University of California

Berkeley, California 94720

In order to illustrate the physical meaning of the four independent interdiffusion coefficients which describe a single phase ternary system, a range of concentration profiles and diffusion paths for the generalized diffusion couple A 10 wt.% B -- A 10 wt.% C were plotted, using three different models of diffusion coefficient behavior. The shapes of the diffusion paths predicted by these various models were compared with that of an experimentally determined diffusion path from the cobalt solid solution of the substitutional alloy system cobalt-chromium-aluminum. The results indicate that even the most sophisticated dilute solution model fails to predict completely the behavior of the real system.

*Shell Research Center, Thornton, Near Chester, England.

1. INTRODUCTION

When interdiffusion coefficients are quoted for a multicomponent system under a particular set of conditions, it is often difficult to appreciate the physical significance of those coefficients. It is, therefore, useful to know how the shape of a concentration profile varies with changes in the values of the coefficients describing the profile. In a binary system, the diffusion behavior can be described by a single independent interdiffusion coefficient. Thus, providing that some simple model exists for the way that the coefficient varies with composition, it is comparatively easy to deduce the composition at some point in a binary system after a particular diffusion treatment. Typically, the diffusion coefficient is assumed to be independent of composition and the concentration profile can then be expressed as a simple error function solution. The concentration profiles produced as a result of binary diffusion into and out of a variety of geometrical shapes have been studied extensively by Crank,(1) who has shown how the value of the diffusion coefficient affects such profiles.

For a ternary system, however, the problem of deducing the shape of concentration profiles from the values of coefficients is much more complex. This is because four independent coefficients are needed to describe ternary diffusion, each of which will probably show a different variation with composition. It is proposed here to develop equations for concentration profiles, and hence show how those profiles appear when plotted for each of a number of assumptions as to the ways in which the various coefficients vary with composition.

Consider a ternary system comprising three elements A, B and C. Suppose now that an infinite diffusion couple is constructed from two different single phase alloys of the A-B-C system, and that element A is the majority element, or solvent, in each case. The two alloys concerned have compositions C_A^- wt.% A-C_B^- wt.% B-C_C^- wt.% C and C_A^+ wt.% A-C_B^+ wt.% B-C_C^+ wt.% C respectively and it is assumed that the ends of the couple retain these compositions throughout the subsequent diffusion anneal.

The diffusion behavior of B and C are described by the generalized form of Fick's 2nd Law for a ternary system, as shown in equations (1) and (2):

$$\frac{\partial C_B}{\partial t} = \frac{\partial}{\partial x}\left[D_{BB}^{A} \cdot \frac{\partial C_B}{\partial x}\right] + \frac{\partial}{\partial x}\left[D_{BC}^{A} \cdot \frac{\partial C_C}{\partial x}\right] \qquad (1)$$

$$\frac{\partial C_C}{\partial t} = \frac{\partial}{\partial x}\left[D_{CC}^{A} \cdot \frac{\partial C_C}{\partial x}\right] + \frac{\partial}{\partial x}\left[D_{CB}^{A} \cdot \frac{\partial C_B}{\partial x}\right] \qquad (2)$$

- with the boundary conditions defined by equations (3) and (4):

$$C_i = C_i^- \text{ at } \lambda = -\infty \qquad (3)$$

$$C_i = C_i^+ \text{ at } \lambda = +\infty \qquad (4)$$

where i = A, B or C

$$\lambda = \frac{x}{t^{1/2}}$$

D_{BB}^{A} and D_{CC}^{A} are the direct diffusion coefficients in the ternary A-B-C system with A as solvent and represent the influences of the concentration gradients of B and C on the fluxes of B and C, respectively; D_{BC}^{A} and D_{CB}^{A} are the indirect or cross coefficients and represent the influences of the concentration gradients of C and

B on the fluxes of B and C, respectively. (Note the superscript to the diffusion coefficients is henceforth omitted since element A is considered to be the solvent throughout the ensuing analysis.)

In order to solve equations (1) and (2), it is necessary to know the dependence of each coefficient on composition. Initially, it will be assumed that the direct coefficients are constant with composition while the cross coefficients are zero, in which case the solutions of equations (1) and (2) are quite straightforward. Non-zero cross coefficients will be introduced later and it will be seen that these give rise to complications in the equations for the concentration profiles.

CONSTANT DIRECT AND ZERO CROSS COEFFICIENTS

2.1. Solution to Diffusion Equation

If D_{BC} and D_{CB} are negligibly small (effectively zero), while D_{BB} and D_{CC} are independent of composition (and hence also of distance and time), the diffusion coefficients in equations (1) and (2) can be taken outside the differential, and the second terms on the right-hand side neglected. The solutions are then similar to that for a binary system:

$$C_B = C_B^+ + 1/2\ (C_B^- - C_B^+)\ \text{erfc}\ \lambda/\sqrt{2D_{BB}} \qquad (5)$$

$$C_C = C_C^+ + 1/2\ (C_B^- - C_C^+)\ \text{erfc}\ \lambda/\sqrt{2D_{CC}} \qquad (6)$$

Thus, concentration profiles can be obtained. If then the values of C_B are plotted against the values of C_C obtained at the same λ, the diffusion path can also be obtained.

Consider the situation where $D_{BB} = D_{CC} = D$. Equations (5) and (6) can then be combined to give:

$$\frac{(C_B - C_B^+)}{(C_B - C_B^+)} = \frac{(C_C - C_C^+)}{(C_C^- - C_C^+)}$$

or
$$C_B = C_C \frac{(C_B^- - C_B^+)}{(C_C^- - C_C^+)} + (C^+ - C^+) \frac{(C_B^- - C_B^+)}{(C_C^- - C_C^+)} \qquad (7)$$

Thus, under these circumstances, the diffusion path is a straight line of gradient $(C_B^- - C_B^+) / (C_C^- - C_C^+)$. This situation is analogous to a binary system because the two species, B and C, are behaving as though they were one. Because there is no chemical interference between the two species, there are no cross coefficients and the two direct coefficients are identical.

When the two direct coefficients are not equal, the diffusion path is not a straight line. Equations (5) and (6) will now be used to investigate the shape of the diffusion path at various values of the diffusion coefficients.

2.2 Theoretical Profiles

Although the concentration profiles depend on the actual values of both direct coefficients, the shape of the diffusion path depends only on the ratio $D_{BB} : D_{CC}$. Therefore, D_{BB} has been held constant

at 10^{-10} cm^2/s and D_{CC} allowed to vary in the range 10^{-11} to 10^{-9} cm^2/s, giving a range of D_{BB}/D_{CC} from 0.1 to 10. The diffusion couple considered for this exercise was one between the alloys A - 10 wt.% B and A - 10 wt.% C and it was assumed that these compositions, and any others arising in the couple, were within the range of the A-rich solid solution, i.e., single phase throughout.

A computer program was used to solve equations (1) and (2) under the conditions given. Theoretically, the concentration profiles extend from $\lambda = -\infty$ to $+\infty$, but a finite range of 10^{-4} to 10^{+4} $cm/s^{1/2}$ was suitable to show the major changes of composition for the range of diffusion coefficients selected. Intervals of λ of 10^{-7} $cm/s^{1/2}$ were deemed suitable to give smooth profiles and diffusion paths. Table I lists the eleven sets of diffusion coefficient data used.

Rather than plot the concentration profiles as functions of λ, the more physically meaningful parameter of distance (x) has been used. Thus, an arbitrary anneal time of 4 days or 345,600 s. was chosen, simply because this was the anneal time employed in obtaining the experimental results referred to in Section 4.

The concentration profiles are shown in Figure 1. Since there are no cross diffusion coefficients operating, the diffusion flux of a particular component is determined solely by the concentration gradient of that component together with the appropriate direct diffusion coefficient. Hence, the profile of B is the same for all eleven sets of conditions because D_{BB} is considered invariant. However, as may be seen, the C profile varies considerably with the value of D_{CC}.

The steepest C profile corresponds to $D_{CC} = 10^{-11}$ cm^2 sec^{-1}, then as D_{CC} increases the profiles become less steep.

It is to be noted that at all values of D_{CC}, the C profile is symmetrical about the point 5%C. Thus, the Matano Interface remains fixed at the position of the original weld of the two halves of the diffusion couple (x = 0). This happens because assumptions, which do not allow for the existence of a Kirkendall Effect, are made in deriving this simple analytical solution of the diffusion equation.

As may be expected, when $D_{CC} = 10^{-10}$ cm^2 sec^{-1}, i.e., equal to D_{BB}, the C profile is symmetrical with the B profile, thus the combined concentration profile ($C_B + C_C$) is a horizontal straight line. Furthermore, the diffusion path (Fig. 2) corresponding to this couple is a straight line from A-10%B to A-10%C. This is all in accordance with equation (7) and the observation made then that when $D_{BB} = D_{CC}$ the system behaves as a pseudo-binary.

It is seen from the diffusion path diagram that the deviation from a straight line, of the path corresponding to $D_{CC} = 10^{-11}$ cm^2 sec^{-1} is the same (in degree) as that when $D_{CC} = 10^{-9}$ cm^2 sec^{-1}. In the first case $D_{BB}/D_{CC} = 10$, while in the second $D_{CC}/D_{BB} = 10$, and this illustrates the point that it is the ratio of the direct coefficients and not their absolute values which determines the shape of the diffusion paths.

3. CONSTANT DIRECT AND CONSTANT CROSS COEFFICIENTS

The curves produced in the previous section are useful in that they demonstrate the effect of direct coefficients in isolation, but in virtually all real ternary systems there is some chemical interaction between the two solute elements which manifests itself in the form of cross diffusion coefficients. Finite cross coefficients complicate the solution of the diffusion equation and, in addition, it becomes necessary to know how the cross coefficients vary with composition. Initially, the situation will be considered in which the cross coefficients are independent of composition.

3.1 Solution to Diffusion Equation

The complete solutions of equations (1) and (2) with constant direct and constant cross coefficients were first given by Fujita and Gosting (2) and are unmanagably complex. To simplify matters, the situation will be considered in which D_{CB} is zero. Thus, the solution to equation (2) is simply equation (7) as considered previously. The solution to equation (1) meanwhile becomes:

$$C_B = \frac{(C_B^+ + C_B^-)}{2} + \frac{(C_B^+ - C_B^-)}{2} \cdot \operatorname{erf} \frac{\lambda}{2\sqrt{D_{BB}}} + \frac{(C_C^- - C_C^+)}{2} \cdot \frac{D_{BC}}{(D_{BB}-D_{CC})}$$

$$\cdot \left[\operatorname{erf} \frac{\lambda}{2\sqrt{D_{CC}}} - \operatorname{erf} \frac{\lambda}{2\sqrt{D_{BB}}} \right] \qquad (8)$$

The first two terms in this expression are just the solution for C_B when D_{BC} is zero (equation 6), while the third term (T) takes account of the cross diffusional effect.

Consider solution (8) when $D_{BB} = D_{CC}$. Under these circumstances T becomes indeterminate, but a limiting solution can be found by using L'Hôpital's rule:

$$\lim_{D_{BB} \to D_{CC}} \left[\frac{(\mathrm{erf}\lambda/2\sqrt{D_{CC}} - \mathrm{erf}\lambda/2\sqrt{D_{BB}})}{(D_{BB} - D_{CC})} \right]$$

$$= \lim_{D_{BB} \to D_{CC}} \left[\frac{\partial/\partial D_{BB} \cdot (\mathrm{erf}\lambda/2\sqrt{D_{CC}} - \mathrm{erf}\lambda/2\sqrt{D_{BB}})}{\partial/\partial D_{BB} \cdot (D_{BB} - D_{CC})} \right]$$

$$= - \frac{(\mathrm{erf}\lambda/2\sqrt{D_{BB}})}{\partial D_{BB}}$$

$$= \frac{\lambda}{2\pi^{1/2} D_{BB}^{3/2}} \cdot \exp \left[\frac{-\lambda^2}{4D_{BB}} \right]$$

Thus,

$$\lim_{D_{BB} \to D_{CC}} T = - \frac{(C_C^+ - C_C^-)}{2} \cdot \frac{D_{BC}}{2\pi^{1/2} D_{BB}^{3/2}} \cdot \lambda \cdot \exp \left[\frac{-\lambda^2}{4D_{BB}} \right]$$

and for the case where $D_{BB} = D_{CC}$ and $D_{CB} = 0$, the solution for the concentration profile of B becomes:

$$C_B = \frac{(C_B^+ + C_B^-)}{2} + \frac{(C_B^+ - C_B^-)}{2} \cdot \text{erf} \frac{\lambda}{2\sqrt{D_{BB}}} - \frac{(C_C^+ - C_C^-)}{2}$$

$$\cdot \frac{D_{BC}}{2\pi^{1/2} D_{BB}^{3/2}} \cdot \lambda \cdot \exp \left[\frac{-\lambda^2}{4D_{BB}} \right]$$

3.2 Theoretical Profiles

These solutions have been used to produce a number of concentration profiles and diffusion paths to show the effect of cross coefficients.

3.2.1 Direct Coefficients equal to each other

Initially, the direct coefficients, D_{BB} and D_{CC}, were set equal to each other so that the effect of the cross coefficient would be highlighted. This is so because any deviation from symmetry between the B and C concentration profiles, and any deviation of the diffusion path from a straight line, can be attributed directly to the cross effect. Twelve different solutions were evaluated using the diffusion coefficient data shown in Table 2.

As previously, a couple between A-10%B and A-10%C was considered, and results computed from $\lambda = -5 \times 10^{-5}$ to $\lambda = 5 \times 10^{-5}$ cm/s$^{1/2}$, which are presented as functions of distance using an anneal time of 4 days (345,600 s).

The concentration profiles are plotted in Figure 3, from which it can be seen that the higher the value of D_{BC}, the greater the deviation of the B profile from its symmetry with the C profile. Again, this model allows no movement of the Matano Interface from the original weld position. It is seen from the concentration profiles, and indeed

the diffusion paths (Fig. 4), that the introduction of a constant cross coefficient of sufficient magnitude results in a maximum and a minimum in the B profile. Thus, the concentration of B has gone outside the bounds of the original alloys making up the couple. The presence of the maximum is quite feasible and merely illustrates the "uphill" diffusion which can occur when cross coefficients are operating. When the diffusion flux of one component depends partly on the concentration gradients of the other elements, then it is possible for that component to diffuse up its own concentration gradient under certain circumstances. The minimum in the B profile, however, is erroneous since it suggests that the concentration of B can become negative. This situation arises because of the assumption that D_{BC} is constant with composition, and the case considered here clearly demonstrates the invalidity of this assumption. However, Kirkaldy (3) has suggested that the assumption of constant cross coefficients is reasonable in circumstances in which the overall change in composition is no more than 20% of the average composition. Thus, a diffusion couple between (say) A-11%B-9%C and A-9%B-11%C would just satisfy Kirkaldy's condition with respect to both B and C.

An interesting observation on the effect of the cross coefficient is that it has only a very slight effect on the width of the region over which significant diffusion takes place. This may be contrasted with the effect of varying the direct coefficient by referring back to Fig. 1 where very substantial broadening of the diffusion zone was effected by increasing D_{CC}. The reason for the difference is that the cross effect on the B profile at any point depends on the concentration

gradient of the C profile at that point, which in turn is determined solely by the value of D_{CC}. Since the C profile extends approximately over the range -75μm to +75μm (Fig. 3), this is the approximate limit of the cross effect on the B profile. A corollary of this is that if the C profile is broadened by increasing D_{CC}, then the range of the effect of the cross term on the B profile is increased.

In order to illustrate this effect, and also to demonstrate the use of solution (9), the situation will now be considered in which D_{BB} and D_{CC} are not equal to each other.

3.2.2 Direct Coefficients different from each other

Another set of concentration profiles and diffusion paths were produced using the diffusion coefficient values shown in Table 3.

The only difference between these and the data used in Section 3.2.1 is that D_{CC} has been changed so that it is no longer equal to D_{BB}.

As before, the solution for the C profile is given by equation (8), but the B profile is now given by equation (7).

The concentration profiles and diffusion paths for the data in Table 3 are shown in Figs. 5 and 6, respectively. It is seen from Fig. 5 that at any particular value of the cross coefficient, D_{BC} (especially at the highest values), the broadening of the component B diffusion zone by the cross effect is much greater than that of the respective profile in Fig. 3. This may be understood by remembering that the cross effect on the B profile at any point is a function of the concentration gradient of C at that point.

An important difference between the B profiles in Fig. 5 and those in Fig. 3 is that, for any value of D_{BC}, the height of the maximum above the adjacent terminal composition and the corresponding depth of the minimum are smaller in the former case than in the latter. This can be traced back to changes in the C profile. Because D_{CC} is larger in Fig. 5 than in Fig. 3, the C profile is generally less steep, i.e., the concentration gradient of C at any point is less. Now, the cross effect on the B profile depends not only on the value of D_{BC}, but also on that of $\partial C_C/\partial x$. Therefore, in Fig. 5, where $\partial C_C/\partial x$ is less, a smaller cross effect on the B profile is observed. This clearly illustrates the important point that it is not merely the diffusion coefficients which determine the net flow of matter in an inhomogeneous system.

Figure 6 shows the diffusion paths corresponding to Fig. 5 and reflects the points already noted. Because D_{CC} is not equal to D_{BB} the diffusion path is not a straight line when $D_{BC} = 0$ (cf. Fig. 4), but is a curve --------- identical, in fact, to the diffusion path corresponding to $D_{BB} = 10^{-10}$ cm^2 sec^{-1}, $D_{CC} = 4 \times 10^{-10}$ cm^2 sec^{-1} on Fig. 2.

In most real ternary systems, both cross diffusion coefficients are significant and are involved in shaping concentration profiles and diffusion paths. The complete solution to the diffusion equation under these circumstances is given by Fujita and Gosting (2) and is very involved because it is necessary to take account of a double coupling effect between the two independent components. The cross effect on the B profile depends on the C concentration gradient, which

itself depends on a cross effect, but this depends on the B concentration profile, which in turn depends on the original cross coefficient, etc. It would be difficult to interpret theoretical diffusion profiles in terms of this involved interrelationship. In any case, even if interpretation were to prove possible, no new basic principles would be illustrated and, therefore, this model will not be considered here.

4. CONSTANT DIRECT AND VARIABLE CROSS COEFFICIENTS

The prediction of negative concentrations renders unreasonable the assumption that all four diffusion coefficients are constant with composition for the diffusion couple A-10% B/A-10% C. Therefore, it is necessary to look for a suitable model to define the variations of the four coefficients with composition. This has been attempted by Bolze, Coates and Kirkaldy (4), who came to the conclusion that, for dilute solutions, the direct coefficients D_{BB} and D_{CC} can be reasonably represented by average constants, while, to the first order in concentration, the cross coefficients can be described by the following equations:

$$\frac{D_{BC}}{D_{BB}} = \alpha_{BC} C_B \tag{10}$$

$$\frac{D_{CB}}{D_{CC}} = \alpha_{CB} C_C \tag{11}$$

where α_{BC} and α_{CB} are proportionality constants closely related to the so called Wagner Interaction Parameters. In his model for the relationships between activity coefficients and composition in a ternary system ABC, which is dilute with respect to B and C, Wagner (5) defines the following interaction parameters:

$$\varepsilon_{BB} = \left[\frac{\partial \ln \gamma_B}{\partial N_B}\right]_{N_A \to 1} \quad , \quad \varepsilon_{BC} = \left[\frac{\partial \ln \gamma_B}{\partial N_C}\right]_{N_A \to 1}$$

$$\varepsilon_{CB} = \left[\frac{\partial \ln \gamma_C}{\partial N_B}\right]_{N_A \to 1} \quad , \quad \varepsilon_{CC} = \left[\frac{\partial \ln \gamma_C}{\partial N_C}\right]_{N_A \to 1}$$

Where γ_B and γ_C are the Activity Coefficients of B and C, respectively. N_B and N_C are the Atomic Fractions of B and C, respectively.

Hence, the activity coefficients are related to composition according to:

$$\ln \frac{\gamma_B}{\gamma_B^o} = \varepsilon_{BB} N_B + \varepsilon_{BC} N_C \qquad (12)$$

$$\ln \frac{\gamma_C}{\gamma_C^o} = \varepsilon_{CC} N_C + \varepsilon_{CB} N_B \qquad (13)$$

where γ_B^o and γ_C^o arise as integration constants and are the Henrian activity coefficients of B and C respectively, which in a real system, not obeying Henry's Law, are the activity coefficients of B and C at infinite dilution. Wagner showed that in the dilute limit (i.e., N_B and $N_C \longrightarrow 0$), then $\varepsilon_{BC} = \varepsilon_{CB}$.

According to Bolze, Coates and Kirkaldy (4), under certain circumstances the factors α_{BC} and α_{CB} in equations (10) and (11) are purely thermodynamic. In particular, when the partial molar volumes and atomic jump frequencies of the three components present are identical (so that the Kirkendall Effect vanishes) than $\alpha_{BC} = \varepsilon_{BC}$ and $\alpha_{CB} = \varepsilon_{CB}$.

4.1 Numerical Solution to Diffusion Equation

The diffusion equations (1) and (2), with D'_{BB} and D_{CC} independent of composition are inhomogeneous, and cannot be solved analytically, although complete numerical solution is possible via an iterative procedure. To simplify the solution procedure, without any great loss of generality, a system for which $D_{CB} = 0$ will again be considered. The solution for C_C is again then given in equation (7).

Substituting this in equation (1) and using equation (10) gives:

$$\frac{\partial C_B}{\partial t} = D_{BB} \cdot \frac{\partial^2 C_B}{\partial x^2} + \frac{\alpha_{BC} \cdot D_{BB}}{\sqrt{\pi D_{CC}\, t}} \cdot \frac{\partial C_B}{\partial x} \cdot \frac{(C_C^{+} - C_C^{-})}{2} \cdot \exp\,(-x^2/4D_{CC}t)$$

$$- \frac{\alpha_{BC} . D_{BB} . x . C_B}{2\sqrt{\pi . D_{CC}^3 . t^3}} \cdot \frac{(C_C^{+} - C_C^{-})}{2} \cdot \exp\,(-x^2/4D_{CC}t) \qquad (14)$$

Equation (20) is now converted to non-dimensional form so that the solution, which will be subsequently developed, may be applicable outside the scope of the current work.

The following dimensionless variables are defined:

$$u = \frac{C_B}{(C_B^{-} - C_B^{+})}$$

$$D_{CC}' = \frac{D_{CC}}{D_{BB}}$$

$$X = \frac{x}{l}$$

$$T = \frac{D_{BB} . t}{l^2}$$

Substituting for C_B, D_{CC}, x, $\partial C_B/\partial x$, $\partial^2 C_B/\partial x^2$, t and $\partial C_B/\partial t$ in equation (14) gives:

$$\frac{\partial u}{\partial T} = \frac{\partial^2 u}{\partial X^2} + \frac{\alpha_{BC}}{\sqrt{\pi D_{CC}{}^3 T^3}} \cdot \frac{\partial u}{\partial x} \cdot \frac{(C_C{}^+ - C_C{}^-)}{2} \cdot \exp\left[\frac{-X^2}{4 D_{CC}' T}\right]$$

$$- \frac{\alpha_{BC} X}{2\sqrt{\pi D_{CC}{}'^3 T^3}} \cdot u \cdot \frac{(C_C{}^+ - C_C{}^-)}{2} \cdot \exp\left[\frac{-X^2}{4 D_{CC}' T}\right]$$

Putting

$$A = \frac{\alpha_{BC}}{\sqrt{\pi D_{CC}'}} \cdot \frac{(C_C{}^+ - C_C{}^-)}{2}$$

$$B = \frac{\alpha_{BC}}{2\sqrt{\pi D_{CC}'^3}} \cdot \frac{(C_C{}^+ - C_C{}^-)}{2} = \frac{A}{2D_{CC}'}$$

$$\frac{\partial u}{\partial T} = \frac{\partial^2 u}{\partial X^2} + \left[\frac{A}{T^{1/2}} \cdot \frac{\partial u}{\partial X} - \frac{BX}{T^{3/2}} u\right] \cdot \exp\left[-\frac{X^2}{4D_{CC}' T}\right] \quad (16)$$

The terms $\partial u/\partial T$, $\partial u/\partial X$ and $\partial^2 u/\partial X^2$ in equation (16) can be replaced by finite difference approximations. X is divided into increments of h, while T is divided into increments of k. The X and T coordinates at any mesh point are given by:

$$X = ih \quad \text{and} \quad T = jk$$

where i and j are integers

The value of the function u at any point X,T is denoted u_{ij}.

The expressions for the above derivatives of u are then:

$$\frac{\partial^2 u}{\partial X^2} = \frac{1}{h^2} \quad (u_{i+1,j} - 2u_{i,j} + u_{i-1,j}) \tag{17}$$

$$\frac{\partial u}{\partial X} = \frac{1}{2h} \quad (u_{i+1,j} - u_{i-1,j}) \text{ [Central Difference]} \tag{18}$$

$$\frac{\partial u}{\partial T} = \frac{1}{k} \quad (u_{i,j+1} - u_{i,j+1} - u_{i,j}) \text{ [Forward Difference]} \tag{19}$$

In determining $\partial u/\partial X$, the Central Difference approximation is used since it is the most accurate. However, the Forward Difference approximation must be used for $\partial u/\partial T$, because the basic information from which the value of u at any X and T is determined is the knowledge of u as a function of X at T = 0.

Substituting equations (17), (18) and (19) into equation (16) gives:

$$u_{i,j+1} = u_{i,j} + r\,(u_{i+1,j} - 2u_{i,j} + u_{i-1,j}) +$$

$$\left[\frac{A\sqrt{r}}{2\sqrt{j}} \cdot (u_{i+1,j} - u_{i-1,j}) - \frac{Bi}{\sqrt{rj^3}} \cdot u_{i,j}\right] \cdot \exp\left[\frac{-i^2 r}{4 D_{CC}\ jk}\right] \tag{20}$$

$$\text{where } r = k/h^2$$

Now, this kind of explicit solution (i.e., one in which one unknown pivotal value of u is expressed directly in terms of known pivotal

values) is not valid when r is greater than 0.5 (6). However, to minimize the number of steps required to reach any particular value of T, and thereby reduce the amount of computation required, it is desirable to have r as high as possible. Therefore, a value of 0.5 is selected for r and, in fact, this choice simplifies equation (20) to

$$u_{i,j+1} = \frac{1}{2} \cdot (u_{i+1,j} + u_{i-1,j}) + \left[\frac{A}{2\sqrt{2j}} \cdot (u_{i+1,j} - u_{i-1,j}) - \frac{Bi\sqrt{2}}{j^{3/2}} \cdot u_{i,j} \right] \cdot \exp\left[\frac{-i^2}{2 D'_{CC} j} \right] \quad (21)$$

4.2 Theoretical Profiles

The solution just developed was used to produce a number of concentration profiles and diffusion paths for the annealed couple A-10%B/A-10%C to show the effect of a non-constant cross coefficient, whose variation with composition is given by equation (10).

4.2.1 Direct Coefficients equal to each other - As with the constant cross coefficient studies, the two constant direct coefficients, D_{BB} and D_{CC}, were set equal to each other initially in order to see the effect of the cross coefficient in isolation. Three solutions were obtained: $D_{BB} = D_{CC} = 10^{-11}$ $cm^2 sec^{-1}$ in each case, with $\alpha_{BC} = 0$, 0.05 and 0.1, respectively. After solution, the dimensionless parameters were re-converted to the original variables x and t, and concentration profiles plotted for an anneal time of 345,600 s. as previously. The three B concentration profiles thus produced are shown in Fig. 7 along

with the concentration profile for component C which was determined analytically at each point from equation (7).

When α_{BC}=0, the B profile is symmetrical with the C profile, as expected, and as α_{BC} increases so does the deviation of the B profile. When α_{BC}= 0.1, $D_{BC} = 10^{-11}$ cm^2 sec^{-1} at C_B = 10%. Therefore, it is to be expected that, in the region of the diffusion couple near the terminal alloy A-10%B, the concentration profile will closely resemble the one produced earlier with $D_{BC} = 10^{-11}$ cm^2 sec^{-1} and constant. Looking at the profile in Fig. 3 corresponding to $D_{BB} = D_{CC} = 10^{-11}$ cm^2 sec^{-1} and $D_{BC} = 10^{-11}$ cm^2 sec^{-1}, this is seen to be the case. The important difference, however, between the constant and variable cross coefficient models is that in the latter there is no prediction of negative concentrations.

Another interesting point to notice about the introduction of a variable as opposed to a constant cross coefficient is that the concentration of B at the position of the original interface (x = 0) no longer remains fixed at a point midway between the terminal compositions, i.e., 5%B. This arises because the B profile is no longer symmetrical about the position x = 0. Since the theory employed to produce these profiles makes the implicit assumptions of constant partial molar volume and constant atomic jump frequencies throughout the system, there can be no Kirkendall Effect. Therefore, the Matano Interface must remain fixed at x = 0 and so the net amount of B lost from the B rich side of x = 0 is the same as the net amount gained by the B poor side. In order to meet this condition with the now unsymmetrical B profile, it is not possible to have C_B = 5% at x = 0.

The diffusion paths corresponding to the above concentration profiles are shown in Fig. 8. The loss of symmetry resulting from the introduction of variable cross coefficients is emphasized by the fact that the various diffusion paths no longer intersect at the composition A-5%B-5%C, but at approximately A-6.7%B-3.3%C.

4.2.2 Direct Coefficients different from each other - For the purposes of comparison with the above concentration profiles and diffusion paths, and also with those produced using constant cross coefficients, it was decided to produce another set of profiles and paths using the variable cross coefficient model.

Again three solutions were considered using α_{BC} = 0, 0.05 and 0.1, but this time different direct coefficients were used: D_{BB} = 10^{-11} cm^2 sec^{-1} and D_{CC} = 4 x 10^{-11} cm^2 sec^{-1}.

The concentration profiles and diffusion paths produced by these computations are shown in Figs. 9 and 10, respectively. In the region of the terminal alloy A-10%B, the extent of the zone of significant redistribution of component B when α_{BC} is finite is approximately double that observed when α_{BC} is zero (Fig. 9). This may be contrasted with the situation in Fig. 7 ($D_{BB} = D_{CC} = 10^{-11}$ cm^2 sec^{-1}) where no significant broadening of the component B diffusion zone was effected by a non-zero value of α_{BC}. This effect is the same as was observed between Figs. 3 and 5 when D_{BC} was considered constant, and in fact the explanation is the same. Although not so obvious as this broadening effect, the increase of D_{CC} from 10^{-11} to 4 x 10^{-11} cm^2 sec^{-1} can also be seen to reduce the height of the maximum in the B concentration profile. Again, this effect is analogous to that observed in the constant

cross coefficient model when D_{CC} was increased, and again the explanation is the same.

Near the other terminal alloy, A-10%C, no broadening of the diffusion zone by the cross effect is observed. In fact, the shapes of the profiles in this region are very similar to those in the respective area of Fig. 7 when $D_{CC} = 10^{-11}$ cm^2 sec^{-1}. This contrasts with the situation prevailing when Figs. 3 and 5 are compared. On Fig. 9, although a non-zero value of the C concentration gradient exists up to about $x = 150\mu m$, no cross effect on the B profile is observed beyond about $x = 75\mu m$ because in that region $D_{BC} = 0$ (equation (18)).

These effects are reflected in the shapes of the respective diffusion paths, shown in Fig. 10, whose intersection point now occurs at about A-7.8%B-3.5%C.

5. SUPERPOSITION OF THEORETICAL AND EXPERIMENTAL DIFFUSION PATHS

Three different models of varying complexity have so far been described for interdiffusion in a single phase ternary system, using the example of an infinite diffusion couple between A-10%B and A-10%C for the purpose of illustration. It is of interest to know how closely these various models come to describing the diffusion behavior of a real ternary system. For this purpose, an experimentally measured diffusion path from the cobalt solid solution of the substitutional alloy system cobalt-chromium-aluminium (7) has been plotted on the same diagram as the paths which would be predicted by the various theoretical models described earlier. The experimental diffusion path was determined by electron probe X-ray microanalysis of the concentration

profiles across an infinite couple between the alloys Co 11.1 wt.% Cr and Co 3.0 wt.% Cr 5.3 wt.% Al after a 4 day anneal at 1100°C.

The diffusion coefficient data used to generate the theoretical diffusion paths were obtained by estimating values for the particular composition range from experimentally determined diffusion coefficients (7).

$D_{CrCr} = 1.5 \times 10^{-11}$ cm^2 sec^{-1}

$D_{AlCr} = 0$

For all theoretical models considered.

For the 1st model: $D_{CrAl} = 0$

For the 2nd model: $D_{CrAl} = 1.0 \times 10^{-11}$ cm^2 sec^{-1} (constant)

For the 3rd model: $D_{CrAl} = \alpha_{CrAl} \cdot D_{CrCr} \cdot C_{Cr}$

where $\alpha_{CrAl} = 0.1$ (constant)

Because the value of D_{AlAl} is known to vary significantly across the composition range of interest, two different values were selected for investigation:

(1) $D_{AlAl} = 2.0 \times 10^{-11}$ cm^2 sec^{-1}

(2) $D_{AlAl} = 5.0 \times 10^{-11}$ cm^2 sec^{-1}

Thus, two graphs showing the superposition of experimental and theoretical diffusion paths were produced, one for each value of D_{AlAl}; these are shown in Figs. 11 and 12, respectively. It was not possible to carry out a similar superposition of concentration profiles because the origin of x (or λ) is not rigorously defined in the case of the experimental data, the need for locating the Matano Interface having been obviated by the use of the modified form of the Boltzmann-Matano analysis (8).

The theoretical paths were produced as described earlier for each individual model. Because D_{AlCr} was considered to the zero throughout, only one solution for the concentration profile of aluminium was required, for which equation (7) was used. For the first model, equation (6) was used for the chromium concentration profile, while for the second model equation (10) was used, i.e., the form of solution applicable when D_{CrCr} and D_{AlAl} are not equal to each other. For the third model, in which D_{CrAl} is considered to be proportional to the chromium concentration, the finite difference approximation technique was used as before.

Examination of Fig. 12 reveals that in the low chromium-high aluminium region, good agreement is obtained between the experimental and all three theoretical paths, but especially the one derived using a variable value for D_{CrAl}. However, at compositions of greater than approximately 5%Cr, there is substantial divergence between theory and experiment. The introduction of a non-zero value of D_{AlCr} would not improve the "fit" in this region because, according to the theory of Bolze, Coates and Kirkaldy (4), as the aluminium concentration approaches zero so does D_{AlCr}. Hence, it is deduced that it is the assumption of constant direct coefficients which results in good agreement between theory and experiment over part of the composition range, but not over the rest. This deduction is verified by the appearance of Fig. 11 where the lower value of D_{AlAl} has been used. Here, agreement between the experimental path and the theoretical one produced by assuming zero cross coefficients is poor, but for the other two theoretical models, especially the one with a variable value of D_{CrAl}, agreement with experiment is good in the high chromium-low aluminum range (down to about 8%Cr, in fact).

These observations confirm the conclusion reached in reference (7) that the results obtained from the experiments with diffusion couples, in the cobalt solid solution range of the cobalt-chromium-aluminium system, do not conform to even the best theoretical dilute solution approximation. The theory of Bolze, Coates and Kirkaldy, which describes the dependence of the diffusion coefficient matrix of a ternary system on composition, is the most sophisticated currently available. This theory has been shown (9,10) to be successful in describing dilute ternary systems in which one of the alloying elements is interstitial. However, for the system considered above, and possibly also for other substitutional alloy systems, this theory is only valid over narrow composition ranges. This would suggest that the Wagner dilute solution model (5) of the relationship between activity coefficients and composition (as described by equations (20) and (21) (5) is oversimplified for the purposes of general application. A better understanding of the variations of diffusion coefficients with composition awaits a more detailed thermodynamic model than that supplied by Wagner.

ACKNOWLEDGEMENT

This work was performed whilst the authors were at the University of Liverpool and was supported by the Science Research Council. One of us (GWR) also acknowledges the award of an SRC Research Studentship. It is being published with the assistance of the Division of Materials Sciences, Office of Basic Energy Sciences, U.S. Department of Energy under contract No. W-7405-ENG-48.

REFERENCES

1. J. Crank, "Mathematics of Diffusion," Oxford University Press (1956).
2. H. Fujita and L. J. Gosting, J. Am. Chem. Soc., 78 (1956), 1099.
3. J. S. Kirkaldy, Advances in Materials Research, 4, (1970), 55.
4. G. Bolze, D. E. Coates and J. S. Kirkaldy, Trans A.S.M., 62 (1969), 794.
5. C. Wagner, "Thermodynamics of Alloys," Addison-Wesley (1952).
6. G. D. Smith, "Numerical Solution of Partial Differential Equations," Oxford University Press (1965).
7. G. W. Roper and D. P. Whittle, Metals Science J., 14 (1980) 21.
8. G. W. Roper and D. P. Whittle, Scripta Met., 8 (1974), 1357.
9. J. S. Kirkaldy and G. R. Purdy, Can. J. Phys., 40 (1962), 208.
10. L. C. Brown and J. S. Kirkaldy, Trans. A.I.M.E., 230 (1964), 223.

FIGURE CAPTIONS

Figure 1. B and C Concentration Profiles across the Diffusion Couple A 10wt.% B - A 10wt.% C after a 4 day anneal with Constant Direct Coefficients ($D_{BB} = 10^{-10}$ cm^2 sec^{-1}, $D_{CC} = 10^{-11}$ to 10^{-9} cm^2 sec^{-1}) and Zero Cross Coefficients. Full details of Diffusion Coefficient Data are shown in Table 1.

Figure 2. Diffusion Paths corresponding to the B and C Concentration Profiles shown in Fig. 1.

Figure 3. B and C Concentration Profiles across the Diffusion Couple A 10wt.% B - A 10wt.% C after a 4 day anneal with Constant and Equal Direct Coefficients ($D_{BB} = D_{CC} = 10^{-11}$ cm^2 sec^{-1}) and Constant Cross Coefficients (D_{BC} = 0 to 2 x 10^{-11} cm^2 sec^{-1}, $D_{CB} = 0$). Full details of Diffusion Coefficient Data are shown in Table 2.

Figure 4. Diffusion Paths corresponding to the B and C Concentration Profiles shown in Fig. 3.

Figure 5. B and C Concentration Profiles across the Diffusion Couple A 10wt.%B - A 10Wt.% C after a 4 day anneal with Constant and Unequal Direct Coefficients ($D_{BB} = 10^{-11}$ cm^2 sec^{-1}, $D_{CC} = 4 \times 10^{-11}$ cm^2 sec^{-1}) and Constant Cross Coefficients ($D_{BC} = 0$ to 2×10^{-11} cm^2 sec^{-1}, $D_{CB} = 0$). Full details Diffusion Coefficient Data are shown in Table 3.

Figure 6. Diffusion Paths corresponding to the B and C Concentration Profiles shown in Fig. 5.

Figure 7. B and C Concentration Profiles across the Diffusion Couple A 10wt.% B - A 10wt.% C after a 4 day anneal with Constant and Equal Direct Coefficients ($D_{BB} = D_{CC} = 10^{-11}$ cm^2 sec^{-1}) and Cross Coefficients which vary with Composition in accordance with equations (18) and (19) ($_{BC}$ = 0, 0.05 and 0.1, $_{CB}$ = 0).

Figure 8. Diffusion Paths corresponding to the B and C Concentration Profiles shown in Fig. 7.

Figure 9. B and C Concentration Profiles across the Diffusion Couple A 10wt.%B - A 10wt.% C after 4 day anneal with constant and Unequal Direct Coefficients ($D_{BB} = 10^{-11}$ cm^2 sec^{-1}, $D_{CC} = 4 \times 10^{-11}$ cm^2 sec^{-1}) and Cross Coefficients which vary with Composition in accordance with equations (18) and (19) ($\alpha_{BC} = 0$, 0.05 and 0.1, $\alpha_{CB} = 0$).

Figure 10. Diffusion Paths corresponding to the B and C Concentration Profiles shown in Fig. 9.

Figure 11 and Figure 12. Superposition of the Experimentally determined Diffusion Path and the Simulated Diffusion Paths from three different Theoretical Models.

(i) Constant Direct and Zero Cross Coefficients.

(ii) Constant Direct and Constant Cross Coefficients.

(iii) Constant Direct and Variable Cross Coefficients.

(iv) Experimentally Determined Diffusion Path.

Table 1. Diffusion Coefficient Data Used to Plot Theoretical Profiles shown in Figures 1 and 2.

D_{BB} cm^2 sec^{-1}	D_{BC} cm^2 sec^{-1}	D_{CC} cm^2 sec^{-1}	D_{CB} cm^2 sec^{-1}
10^{-10}	0	10^{-11}	0
10^{-10}	0	2×10^{-11}	0
10^{-10}	0	4×10^{-11}	0
10^{-10}	0	6×10^{-11}	0
10^{-10}	0	8×10^{-11}	0
10^{-10}	0	10^{-10}	0
10^{-10}	0	2×10^{-10}	0
10^{-10}	0	4×10^{-10}	0
10^{-10}	0	6×10^{-10}	0
10^{-10}	0	8×10^{-10}	0
10^{-10}	0	10^{-9}	0

Table 2. Diffusion Coefficient Data Used to Plot Theoretical Profiles Shown in Figures 3 and 4.

D_{BB} cm^2 sec^{-1}	D_{BC} cm^2 sec^{-1}	D_{CC} cm^2 sec^{-1}	D_{CB} cm^2 sec^{-1}
10^{-11}	0	10^{-11}	0
10^{-11}	10^{-12}	10^{-11}	0
10^{-11}	2×10^{-12}	10^{-11}	0
10^{-11}	4×10^{-12}	10^{-11}	0
10^{-11}	6×10^{-12}	10^{-11}	0
10^{-11}	8×10^{-12}	10^{-11}	0
10^{-11}	10^{-11}	10^{-11}	0
10^{-11}	1.2×10^{-11}	10^{-11}	0
10^{-11}	1.4×10^{-11}	10^{-11}	0
10^{-11}	1.6×10^{-11}	10^{-11}	0
10^{-11}	1.8×10^{-11}	10^{-11}	0
10^{-11}	2×10^{-11}	10^{-11}	0

Table 3. Diffusion Coefficient Data Used to Plot Theoretical Profiles Shown in Figures 5 and 6.

D_{BB} cm^2 sec^{-1}	D_{BC} cm^2 sec^{-1}	D_{CC} cm^2 sec^{-1}	D_{CB} cm^2 sec^{-1}
10^{-11}	0	4×10^{-11}	0
10^{-11}	10^{-12}	4×10^{-11}	0
10^{-11}	2×10^{-12}	4×10^{-11}	0
10^{-11}	4×10^{-12}	4×10^{-11}	0
10^{-11}	6×10^{-12}	4×10^{-11}	0
10^{-11}	8×10^{-12}	4×10^{-11}	0
10^{-11}	10^{-11}	4×10^{-11}	0
10^{-11}	1.2×10^{-11}	4×10^{-11}	0
10^{-11}	1.4×10^{-11}	4×10^{-11}	0
10^{-11}	1.6×10^{-11}	4×10^{-11}	0
10^{-11}	1.8×10^{-11}	4×10^{-11}	0
10^{-11}	2×10^{-11}	4×10^{-11}	

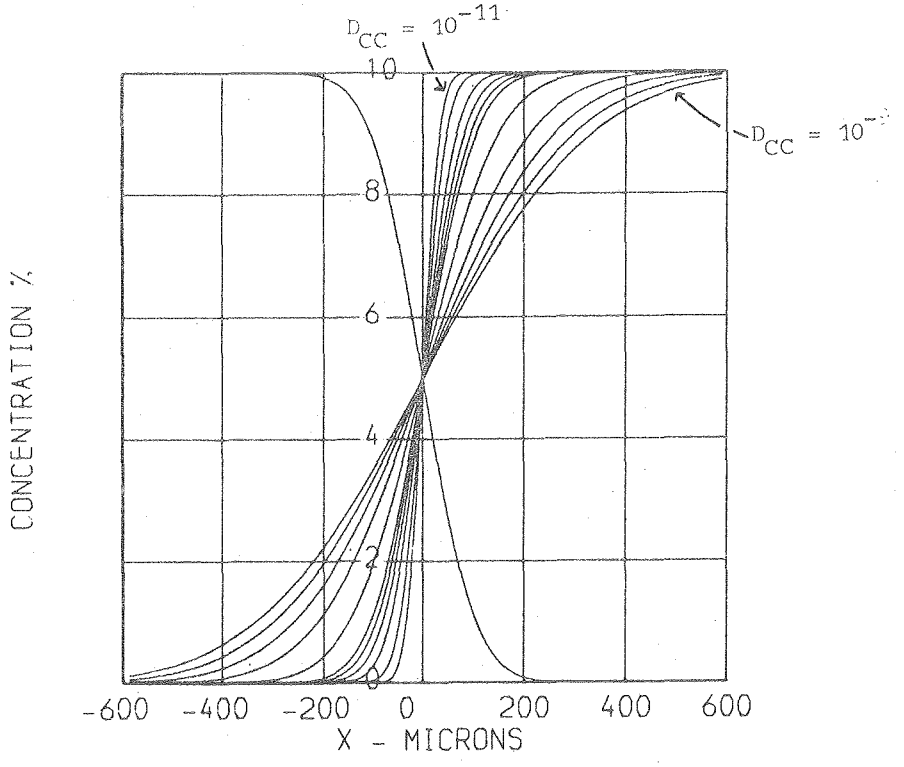

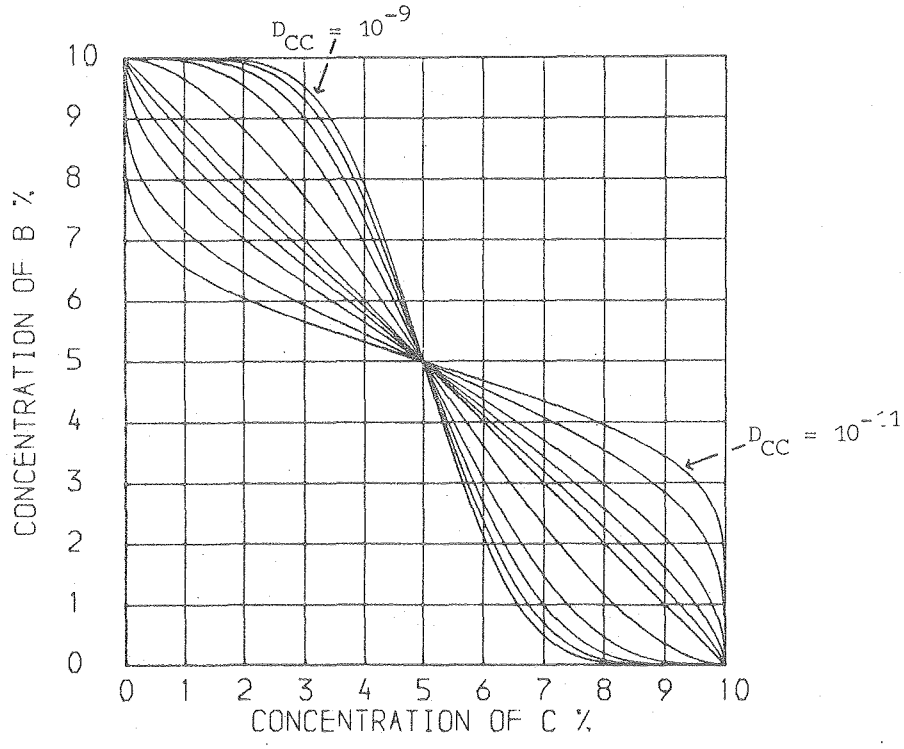

XBL 802-8107

Figures 1 and 2.

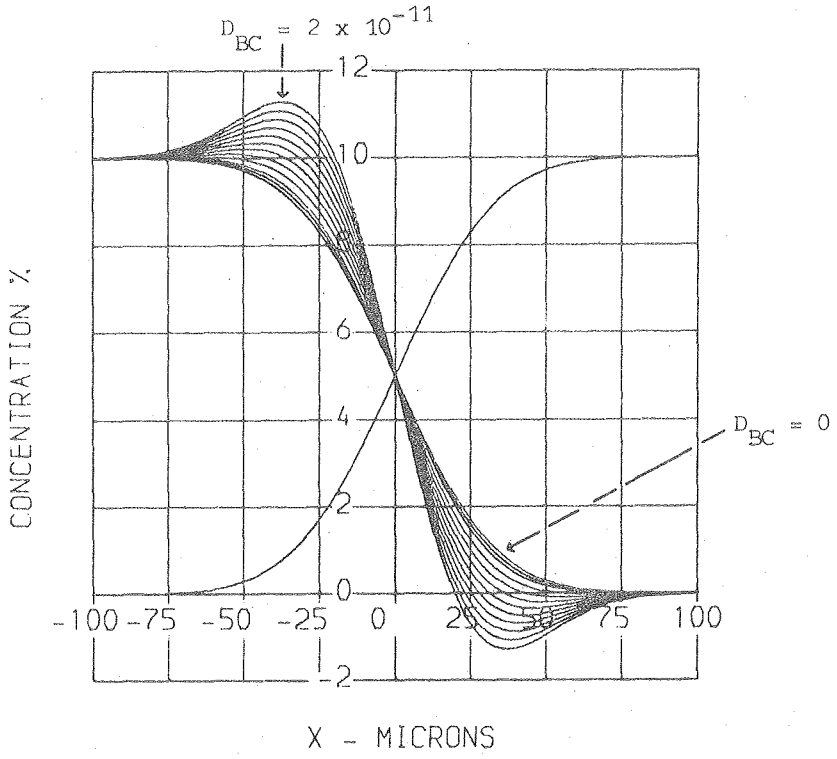

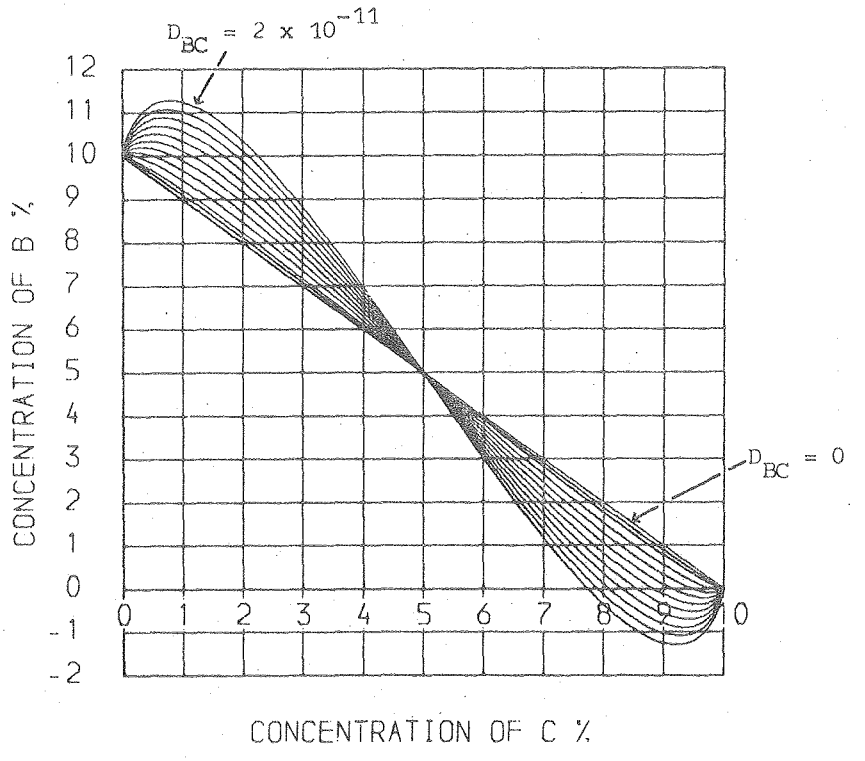

XBL 802-8108

Figures 3 and 4.

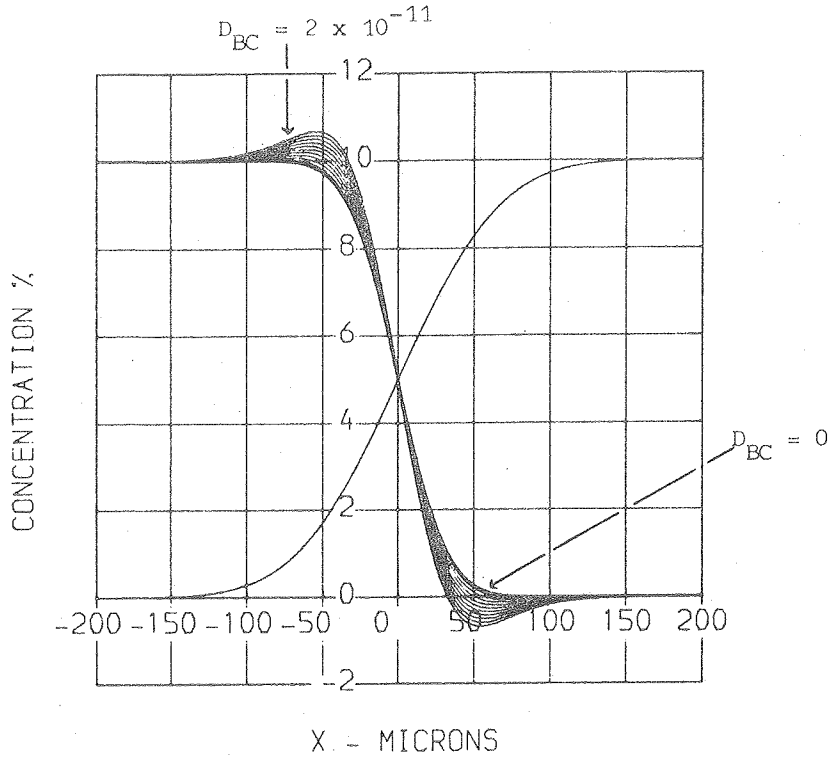

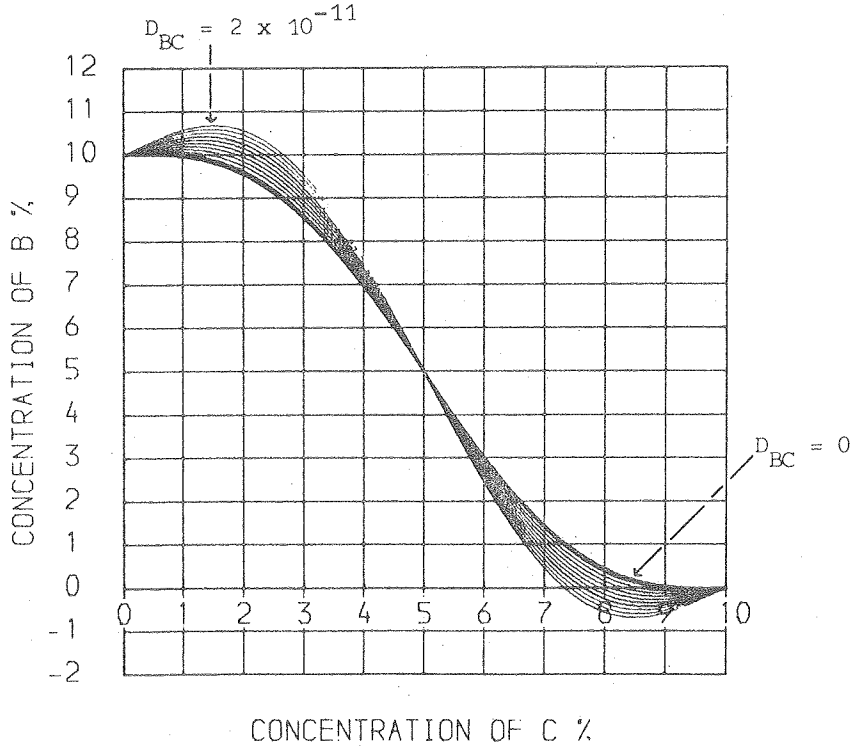

XBL 802-8109

Figures 5 and 6.

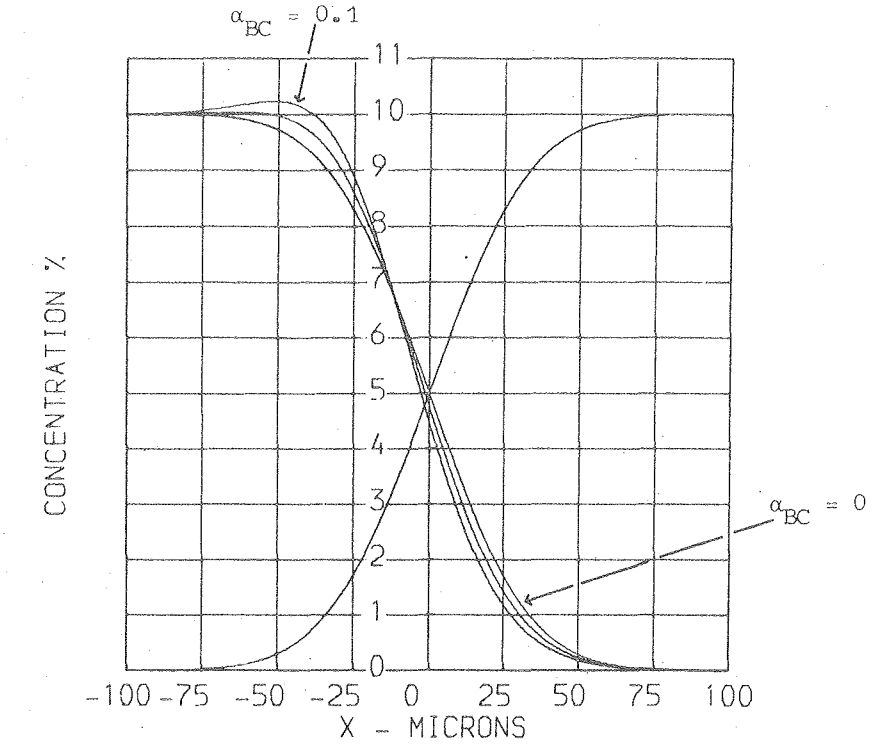

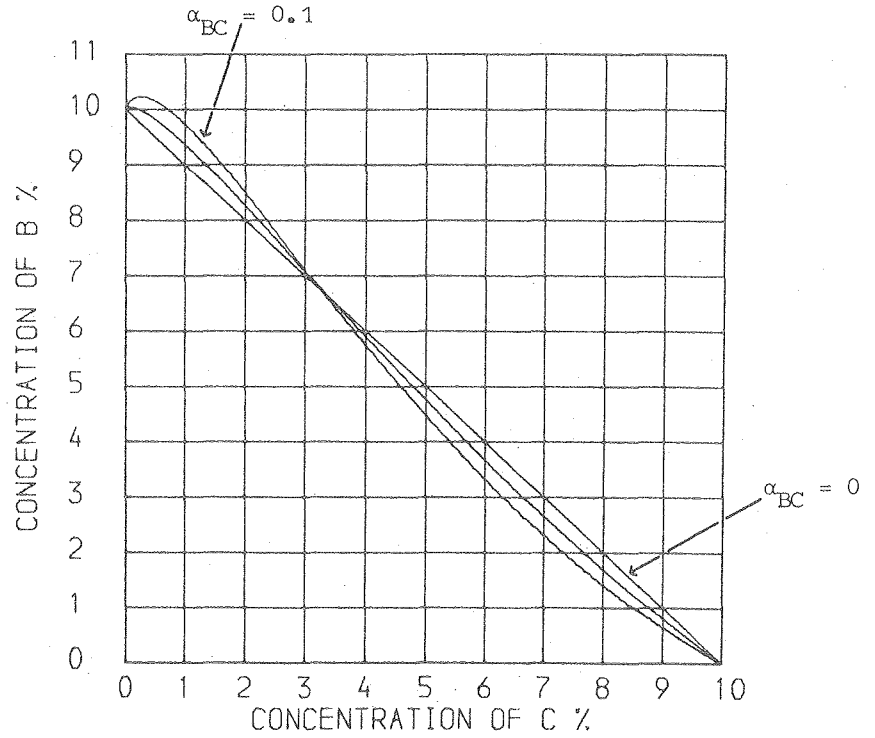

XBL 802-8110

Figures 7 and 8.

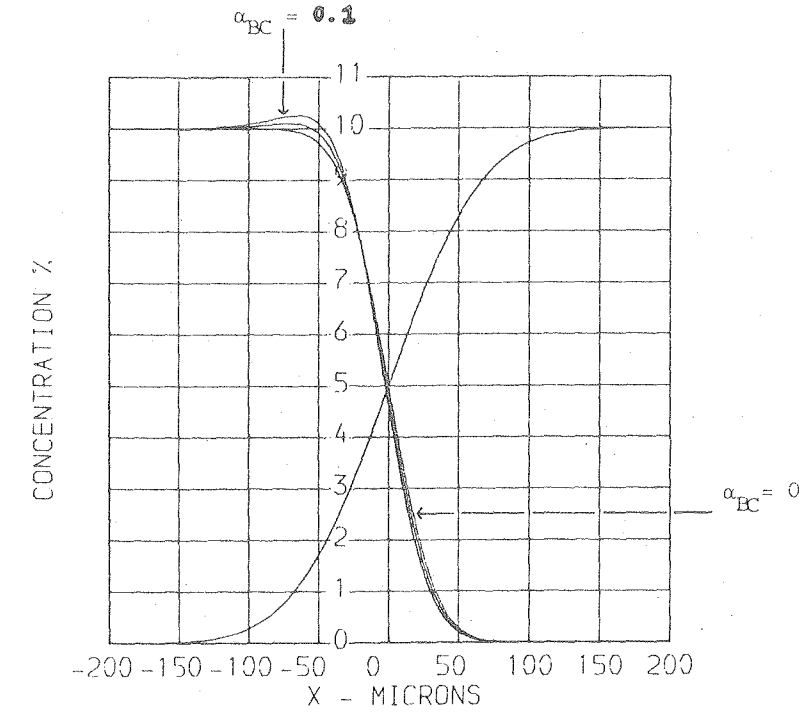

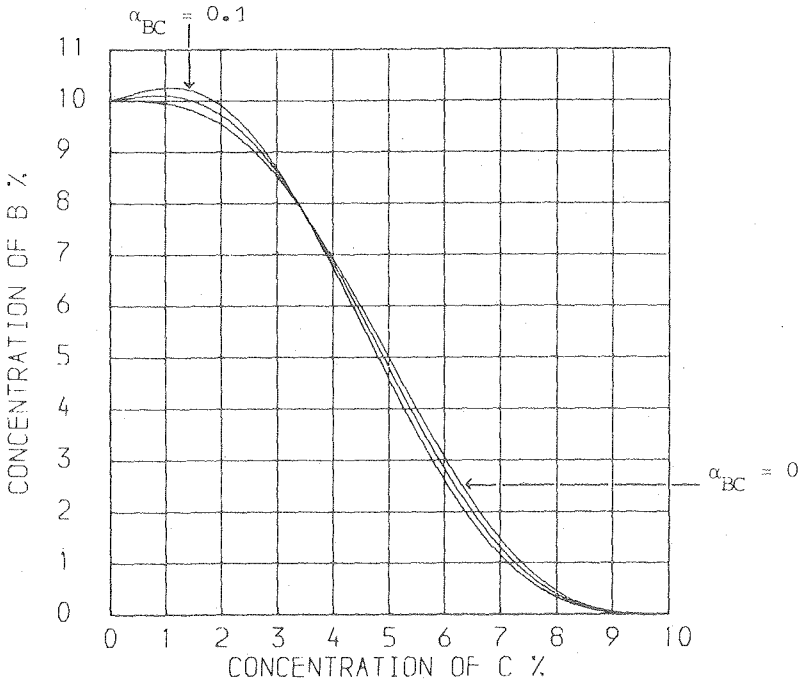

XBL 802-8111

Figures 9 and 10.

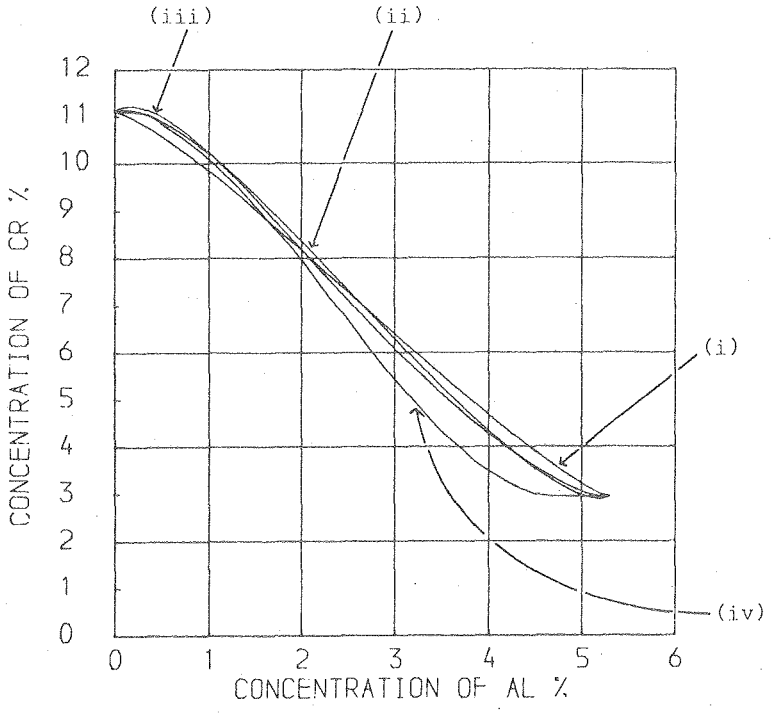

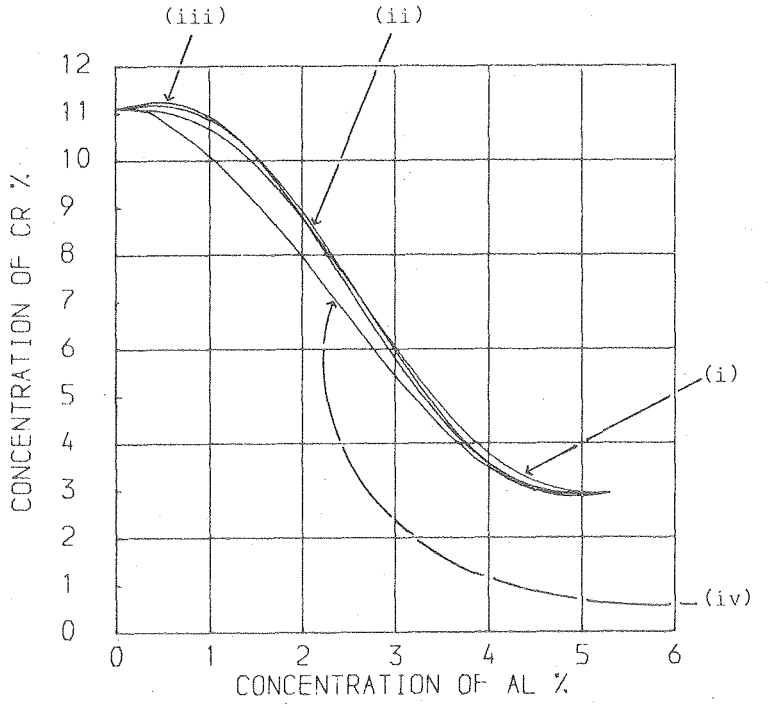

XBL 802-8112

Figures 11 and 12.